Ion irradiation effects on bcc Fe/Tb multilayers

J. Teillet, F. Richomme, and A. Fnidiki
LMA, URA CNRS 808, Faculté des Sciences de Rouen, F-76821 Mont-Saint-Aignan Cédex, France

M. Toulemonde
CIRIL, BP 5133, F-14040 Caen Cédex, France

(Received 22 July 1996)

Fe/Tb multilayers with crystallized Fe layers were irradiated with Kr, Xe, Pb, and U ions at various fluences. Damaging processes, investigated by ^{57}Fe Mössbauer spectrometry at room temperature, give evidence for two thresholds, one for Fe-Tb mixing ($T_1 \sim 25$ keV/nm) and one relative to the creation of defects in the bcc Fe layers ($T_2 \sim 45$ keV/nm). If the electronic stopping power $(dE/dx)_e$ value of ions is less than T_1, only a demixing of Fe and Tb atoms can occur at the interfaces, producing both a thickening of the pure bcc Fe layer and a sharpening of the interfaces whatever the ion fluence is. Between T_1 and T_2, the Fe-Tb demixing is still observed at the lowest fluences, but then the mixing of Fe and Tb layers destroys progressively the layered structure. At high-ion fluences, the samples exhibit the magnetic properties of the corresponding amorphous Fe-Tb alloys. When the energy deposited by the ions exceeds the T_2 value, a third phenomenon appears in addition to the two previous ones: the initial bcc Fe layers are transformed into ''pure'' disordered Fe layers. A qualitative explanation of the evolution versus the ion fluences is proposed using the thermal spike model. [S0163-1829(97)10417-9]

I. INTRODUCTION

Since the 1980s, it has been well established that swift heavy-ion irradiations can induce structural transformations in crystalline and amorphous metallic materials.[1–3] When the energy deposition occurs mainly by electronic interaction with the target, above an electronic stopping power threshold, damages are created into amorphous latent tracks in the ion path.[4,5] In magnetic materials, the structural changes can also produce modifications in the magnetic configuration, such as a reorientation of the magnetic moments along the tracks, as already evidenced in $Y_3Fe_5O_{12}$ (Ref. 6) and YCo_2 (Ref. 7).

Recently, few studies were devoted to multilayered structures. For example, in (bcc Fe/Si) multilayers irradiated with ^{238}U, only a mixing of the Fe and Si layers was observed.[8]

The Fe/Tb multilayers (ML's) are potential candidates for perpendicular magneto-optical recording and it should be very interesting to create a perpendicular magnetic anisotropy (PMA) in crystalline multilayers which initially exhibit an in-plane magnetic anisotropy at room temperature. The aim of this work is to investigate by ^{57}Fe Mössbauer spectrometry at 300 K the structural and magnetic changes produced by ion irradiation in sputtered Fe/Tb ML's. The ^{57}Fe Mössbauer spectrometry is a suitable technique for this kind of investigation because it gives a direct and local characterization of both structural and magnetic states of the iron layers. We reported previously on a detailed diagram of the structural and magnetic properties of the iron layers at room temperature in sputtered Fe/Tb ML's as functions of the iron and terbium layer thicknesses (t_{Fe} and t_{Tb}, respectively).[9] The magnetic properties of these ML's depend strongly on the modulation of composition inside the layers.[9,10] At low Fe thickness, the iron layers are structurally disordered but, from a critical Fe thickness ($t_{Fe} \geqslant 2.2$ nm), iron crystallizes into the bcc structure in the center of the Fe layers.

This paper is dedicated to irradiation effects in two (bcc Fe/Tb) multilayers with t_{Fe} near the limit of crystallization of the Fe layers. The influence of the ion energy deposition on the damages creation is followed varying the energy of the incident ions. The kinetics of the damaging processes are determined using various ion fluences. The results will be correlated with previous ones obtained on irradiated amorphous Fe/Tb multilayers.[11]

II. EXPERIMENT

The ion-irradiation experiments were performed at room temperature in the GANIL accelerator of Caen (France) in the medium-energy line facility which is described elsewhere.[12] This device allows one to irradiate the samples on a large area at a definite temperature with a continuous and homogeneous ion flux. In every case, the samples were mounted with the plane of layers perpendicular to the incident ion beam ($E \approx 1$ GeV).

The Fe/Tb ML's were deposited at room temperature on chemically etched Si(111) substrates using a reactive diode rf-sputtering system. The detailed procedure was reported previously.[9] The entire Fe/Tb stack is always located between two layers of Si_3N_4 (10 nm) in order to prevent corrosion and oxidation. The periodic structure and the layer thicknesses of the nonirradiated films were determined by grazing x-ray diffraction. Their structural and magnetic properties were investigated by high-angle x-ray-diffraction, temperature-dependent conversion electron Mössbauer spectrometry, and magnetization measurements versus temperature and applied magnetic field.[9]

Here, we present the results concerning two multilayers with initial crystalline Fe layers, respectively *S*1 (2.30 nm

TABLE I. Main experimental characteristics and calculated physical parameters (TRIM91) (Ref. 13), R_p is the projected range of ions, $(dE/dx)_e$ and $(dE/dx)_n$ are, respectively, the ion energy loss by electronic excitations and nuclear collisions, ϕ is the fluence of ions. t_{Fe} and t_{Tb} are the nominal iron and terbium thicknesses, X is the mean Tb composition of the ML's.

Sample	t_{Fe} (nm)	t_{Tb} (nm)	X (at. % Tb)	Ions-(MeV/amu) -(MeV)	$(dE/dx)_e$ (keV/nm)	$\frac{(dE/dx)_e}{(dE/dx)_n}$	R_p (μm)	ϕ (10^{12} ions/cm^2)
*S*1	2.30	1.17	15.6	Kr-(10.5) -(819)	16.9	1408	44	6, 16
				Xe-(5.0) -(664)	34.4	702	22	8, 30
				Pb-(4.2) -(870)	52.7	435	23	0.1, 0.5, 1
				U-(3.4) -(810)	55.7	301	21	0.52, 1.76
*S*2	2.70	1.90	20.3	Xe-(7.4) -(960)	31.9	911	32	2, 4, 8

Fe/1.17 nm Tb)$_{75}$ and *S*2 (2.70 nm Fe/1.90 nm Tb)$_{75}$. According to previous results,[9] the Tb layers are amorphous while the Fe layers are crystallized into the bcc structure above the critical iron thickness ($t_{Fec}=2.2$ nm).

The main characteristics of ion irradiation for these two multilayers are listed in Table I. In order to scan the damaging processes, the samples were irradiated with different ions (Kr, Xe, Pb, U) at various fluences in the 10^{11}–3×10^{13} ions/cm^2 range. The total thickness of the Fe/Tb stack is always much smaller than the calculated projected range R_p. Thus, the ions go through the complete (Fe/Tb)$_n$ layered structure. In every case, the calculated electronic and nuclear stopping power values [TRIM91 (Ref. 13)], $(dE/dx)_e$ and $(dE/dx)_n$, respectively, indicate that the defects due to the ion passage come mainly from excitation of the electrons of the target. To reduce thermal effects in the samples, incident ion flux was limited to a few 10^8 ions/cm^2/s.

Before and after irradiation, conversion electron Mössbauer spectrometry (CEMS) experiments were performed at 300 K using a conventional spectrometer equipped with a helium-methane proportional counter at room temperature and a ^{57}Co source in a rhodium matrix. The samples were set perpendicular to the incident γ-beam direction. The Mössbauer spectra were fitted with a least-squares technique[14] using, for the disordered part of iron, the histogram method[15] relative to discrete distributions, constraining the linewidths of each elementary spectrum to be the same. Isomer shifts are given relative to bcc iron at 300 K.

III. RESULTS AND DISCUSSION

A. Nonirradiated multilayers

The two Mössbauer spectra and the hyperfine field distributions $P(B_{hf})$ are drawn in Fig. 1. The Mössbauer spectra exhibit two contributions as evidenced on the $P(B_{hf})$ distributions: the sextet characteristic of α-iron ($B_{hf}=33$ T at 300 K) and a broad component at lower fields. According to a previous study with ^{57}Fe probe layers,[16] this last component is attributed to various environments around the iron sites due to the disordered Fe/Tb interfaces, while the crystallized iron is located in the center of the iron layers.

The mean Mössbauer parameters which are reported in Table II agree with the layered structure. When t_{Fe} increases, the mean isomer shift $\langle IS\rangle$ and the mean hyperfine field $\langle B_{hf}\rangle$ tend towards the values relative to α-iron at 300 K (IS=0 mm/s, $B_{hf}=33$ T). For the two samples, the relative amount of Fe atoms involved at each interface, $1-A_{\alpha\text{-Fe}}$, is equivalent to about two monolayers of iron. Thus, in agreement with the increase of the contribution of α-Fe, the bcc iron layers are thicker for $t_{Fe}=2.70$ nm than for $t_{Fe}=2.30$ nm.

The mean Mössbauer angle β which corresponds to the mean angle between the atomic magnetic moments of iron and the normal to the plane of layers is close to 70°, due to the demagnetizing field relative to the volume which imposes a planar magnetic anisotropy.

B. Irradiated multilayers

1. S1 (2.3 nm Fe/1.17 nm Tb) study

As previously mentioned, the Mössbauer spectrum of the nonirradiated sample *S*1 (Fig. 1) is the sum of a sextet related to bcc Fe (53% of relative spectral area) and a broad-

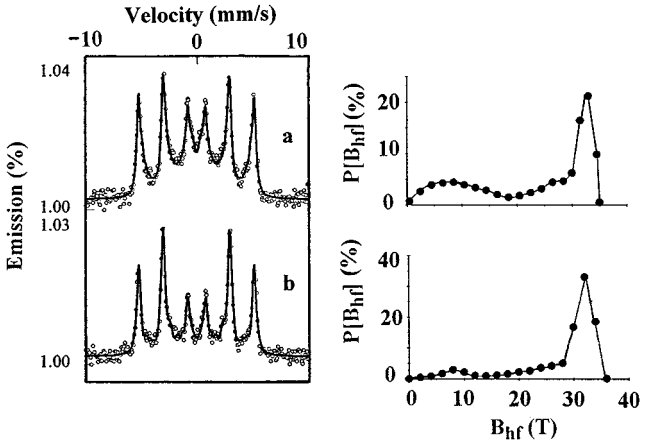

FIG. 1. Mössbauer spectra and hyperfine field distributions $P(B_{hf})$ for the nonirradiated multilayers at 300 K: (a) *S*1 (2.30 nm Fe/1.17 nm Tb); (b) *S*2 (2.70 nm Fe/1.90 nm Tb).

TABLE II. Mean fitted hyperfine parameters of the irradiated Fe/Tb ML's at 300 K. ''No'' refers to the nonirradiated compounds. $\langle IS\rangle$ is the mean isomer shift, $\langle B_{hf}\rangle$ the mean hyperfine field, β the mean Mössbauer angle, $A_{\alpha\text{-Fe}}$ the relative fraction of Fe atoms which are in the bcc iron phase compared to all iron atoms. For comparison, data concerning amorphous Fe-Tb alloys with the same mean global composition are also reported (Refs. 17 and 18).

		Fe/Tb multilayers						Amorphous Fe-Tb alloys	
	X (at. % Tb)	Ions (MeV/amu)	ϕ (10^{12} cm^{-2})	$\langle IS\rangle$ (mm/s)	$\langle B_{hf}\rangle$ (T)	β (deg)	$A_{\alpha\text{-Fe}}$ (%)	$\langle B_{hf}\rangle$ (T)	β (deg)
*S*1	15.7	No	No	−0.011(3)	24.5	68(5)	53	∼15	26
		Kr(10.5)	6	−0.006(3)	27.1	75(4)	57		
			16	−0.005(3)	27.1	77(4)	59		
		Xe(5.0)	8	−0.007(3)	26.9	70(4)	57		
			30	−0.095(6)	13.2	43(5)	3		
		Pb(4.2)	0.1	−0.013(3)	26.5	64(5)	57		
			0.5	−0.008(5)	24.3	77(5)	46		
			1	−0.031(8)	16.8	80(5)	22		
		U(3.4)	0.52	−0.045(5)	21.5	72(4)	42		
			1.76	−0.06(1)	8.6	36(7)	1		
*S*2	20.4	No	No	−0.007(3)	26.0	70(3)	63	18	20
		Xe(7.4)	2	−0.008(3)	26.0	78(3)	54		
			4	−0.009(3)	24.9	86(4)	45		
			8	−0.008(3)	23.2	84(3)	33		

ened contribution due to Fe atoms involved at the interfaces (47% of relative spectral area). This sample is located close to the limit of crystallization of the Fe layers. It was irradiated with four different ions (Kr, Xe, Pb, and U) at various fluences (Table I). The results will be presented separately for each type of ion, increasing the electronic stopping power $(dE/dx)_e$.

(a) Kr ion irradiation. For the two fluences (6×10^{12} ions/cm^2 and 1.6×10^{13} ions/cm^2, Table I), the Mössbauer spectra [Figs. 2(b) and 2(c)] give clear evidence for a decrease of the amorphous part. Such an effect is also shown on $P(B_{hf})$ by a strong decrease of the hyperfine field contributions smaller than 20 T [Figs. 2(b) and 2(c)]. The relative contribution of bcc Fe ($30\leqslant B_{hf}\leqslant 34$ T) increases (Table II) and the mean hyperfine field $\langle B_{hf}\rangle$ increases from 24.5 to 27.1 T (Fig. 3). So it appears clearly that an additional crystallization of iron occurs during the Kr irradiation at these fluences. At the highest fluence (1.6×10^{13} ions/cm^2), the fraction of bcc Fe seems to saturate to a value which is estimated to be 59% instead of 53% initially. This increase of the crystallized part of iron features a thickening of the bcc Fe layers and, consequently, a sharpening of the Fe-Tb interfaces. Such a phenomenon did not appear on (bcc Fe/Si) multilayers.[8] The mean Mössbauer β angle, becoming slightly larger with the fluence (from 68° to 77°) (Fig. 4), indicates that the magnetic iron moments turn more into the film plane. Thus, the increasing planar anisotropy related to the thickening of the bcc Fe layers overtakes the increasing perpendicular magnetic anisotropy produced by the sharpening of the interfaces.

(b) Xe ion irradiation. The fluences are listed in Table I and the Mössbauer spectra are reported in Figs. 2(d) and 2(e).

At the lower fluence (8×10^{12} ions/cm^2), the same induced crystallization of iron, as evidenced for the Kr bombardment, is observed. Due to the increase of the fraction of bcc Fe up to 57% (Table II), the mean hyperfine field $\langle B_{hf}\rangle$ is enhanced from 24.5 up to 26.9 T (Fig. 3). As for the Kr bombardment, the mean Mössbauer β angle seems to increase slightly. Taking into account uncertainties on the β values, no definite conclusion can be given, but it is likely to have the same behavior as for Kr.

At the higher fluence (3×10^{13} ions/cm^2), the usual step of mixing of layers is evidenced. The Mössbauer spectrum and the hyperfine fields distribution are characteristic of a disordered iron alloy. A dramatic increase of the B_{hf} contributions lower than 25 T is observed [Fig. 2(e)], while a strong decrease of the contributions related to bcc Fe ($B_{hf}=30$–34 T) occurs. The $\langle B_{hf}\rangle$ value falls down to 13.2 T (Fig. 3) and the most probable field of $P(B_{hf})$ is only 15 T [Fig. 2(e)]. This last value is very close to the mean hyperfine field of the amorphous Fe-Tb alloy at the same composition (∼15 T for 15–16 at. % Tb).[17,18] All these modifications indicate clearly the destroying of the bcc Fe layers due to the progressive thickening of the Fe-Tb interfaces. The Mössbauer angle dependence follows the same evolution. Decreasing down to 43°, it seems to tend toward the value relative to the corresponding amorphous Fe-Tb alloy (Table II, Fig. 4). From these observations, and because it remains only 3% area fraction of bcc Fe, we conclude that the Fe and Tb layers are nearly completely mixed certainly because of the very high value of the fluence. The mean isomer shift value (Table II) then close to the value of the amorphous Fe-Tb alloy (∼−0.1 mm/s for 15–16 at. % Tb) agrees with a final structure which tends towards an homogeneous amorphous state.

(c) Pb ion irradiation. For the bombardments with Pb ions, three fluences were used (Table I). At the lowest fluence (1×10^{11} ions/cm^2), the additional crystallization of the iron layers is evidenced (up to 57% of bcc Fe) [Fig. 5(b)]. In

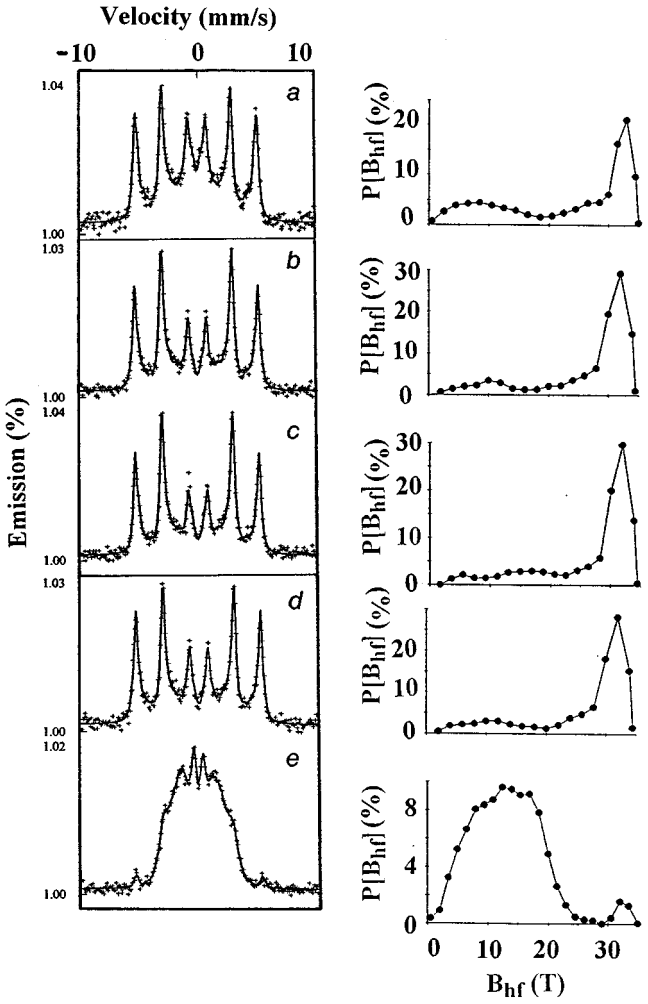

FIG. 2. Mössbauer spectra and $P(B_{hf})$ for the $S1$ sample at 300 K: (a) nonirradiated; (b) 6×10^{12} Kr ions/cm^2; (c) 1.6×10^{13} Kr ions/cm^2; (d) 8×10^{12} Xe ions/cm^2; (e) 3×10^{13} Xe ions/cm^2.

agreement with our previous observations, $\langle B_{hf}\rangle$ is increased up to 26.5 T (Fig. 3). As observed in the Mössbauer angle for the smallest Xe fluence (Table II, Fig. 4), the increase of the bcc Fe part is not enough to produce a meaningful variation of the magnetic anisotropy. At 5×10^{11} ions Pb/cm^2, the mixing of the Fe and Tb layers occurs; $P(B_{hf})$ for the amorphous part exhibits a most probable value near 15 T [Fig. 5(c)], as for the 3×10^{13} ions Xe/cm^2 fluence, and $\langle B_{hf}\rangle$ decreases down to 24.3 T (Fig. 3). At the highest fluence (1×10^{12} ions/cm^2), the bcc Fe contribution has decreased a lot and it remains only 22%. Nevertheless, this vanishing seems to be not due to only the further mixing of the Fe and Tb layers which would lead to a $P(B_{hf})$ analogous to the one of the corresponding Fe-Tb amorphous alloy with a maximum near 15 T. It is noteworthy that the hyperfine field distribution of the amorphous part exhibits a maximum value near 5 T [Fig. 5(d)], i.e., a very low value compared to the $\langle B_{hf}\rangle$ value of the corresponding amorphous Fe-Tb alloy ($\sim$15 T). This weakly magnetic component is also clearly evidenced in the Mössbauer spectrum [Fig. 5(d)]. This is a new phenomenon which never appeared up to now for these

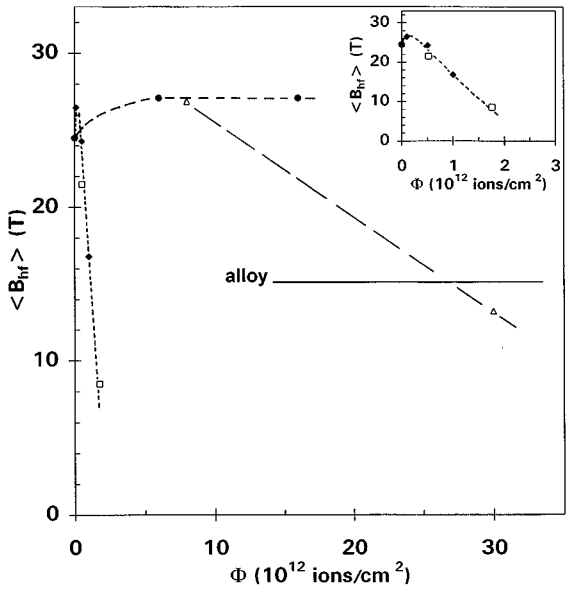

FIG. 3. $\langle B_{hf}\rangle$ vs the ion fluence for the $S1$ sample irradiated with Kr (●), Xe (△), Pb (♦), and U (□) ions. The inset concerns the Pb and U ion irradiations in the low fluence range.

Fe/Tb ML's. As we will see later, it may be correlated with the large $(dE/dx)_e$ value of the concerned Pb ions.

For the two higher fluences, we observe an increase of the mean Mössbauer angle (Table II), so the iron moments rotate towards the layers plane. This effect is in agreement with the mixing of layers which destroys the interfaces and consequently the perpendicular anisotropy. Added to the thickening of the Fe-Tb interfaces, it still exists enough of α-iron in the center of the Fe layers to impose its shape anisotropy.

(d) U ion irradiation. The last investigations were performed at two fluences with U ions having an electronic stopping power value close to the one of the Pb ions (Table I). So, the results were expected to be consistent with those of the Pb irradiation.

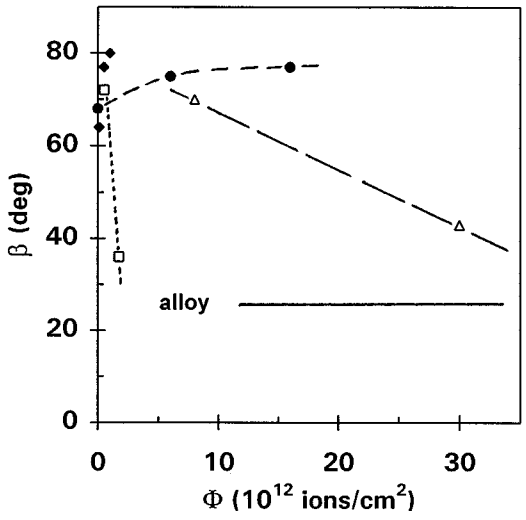

FIG. 4. β as function of the ion fluence for the $S1$ sample irradiated with Kr (●), Xe (△), Pb (♦), and U (□) ions.

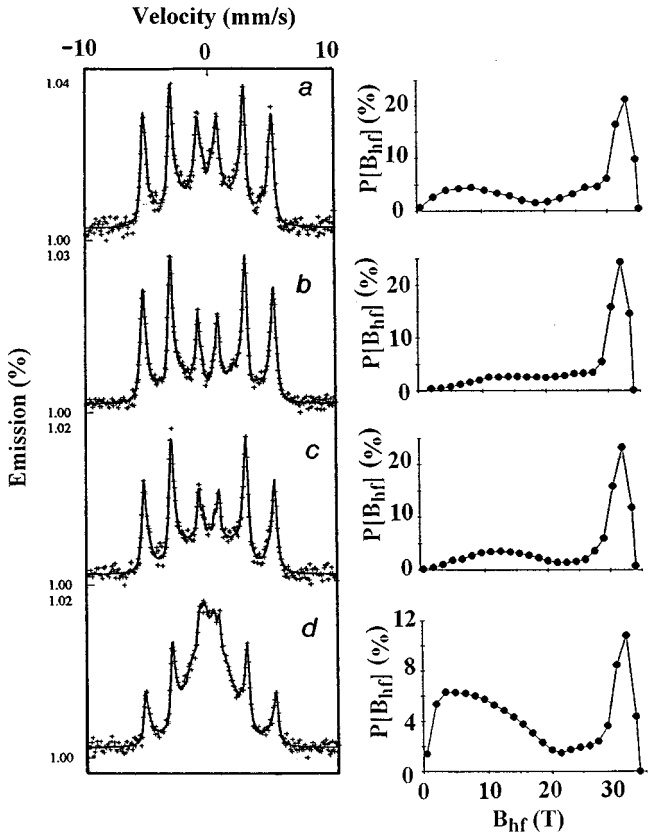

FIG. 5. Mössbauer spectra and $P(B_{hf})$ at 300 K for the $S1$ sample irradiated with Pb ions: (a) nonirradiated; (b) 1×10^{11} ions/cm^2; (c) 5×10^{11} ions/cm^2; (d) 1×10^{12} ions/cm^2.

For the first fluence (5.21×10^{11} ions/cm^2), the results [Fig. 6(b)], and the mean hyperfine field [inset of Fig. 3], are, as expected, between those of the two last fluences of Pb [Figs. 5(c) and 5(d)], already showing on $P(B_{hf})$ the growing of the component located around 5 T. For the fluence of 1.76×10^{12} ions/cm^2, the bcc iron has disappeared [Fig. 6(c)]. The hyperfine field distribution presents a dramatic enhancement of the weakly magnetic phase around 5 T, with an extended tail up to 22 T. The enhancement of the weakly magnetic phase has a strong influence on the mean hyperfine field: $\langle B_{hf}\rangle$ decreases down to 8.6 T (Fig. 3) which is a very low value compared to the one of the corresponding amorphous alloy (15–16 at. % Tb) and the mean Mössbauer angle goes down to 36° (Fig. 4). This value will be discussed later (Sec. III C).

2. S2 (2.70 nm Fe/1.90 nm Tb) study

This sample is farthest off the limit of crystallization of iron. The nonirradiated multilayer presents a larger crystallized bcc iron thickness in the center of iron layer than the previous one.

This multilayer was irradiated only with Xe ions at various fluences (Table I). Increasing the ion fluence, the Mössbauer spectra and hyperfine field distributions (Fig. 7) show a clear decreasing of the contributions between 30 and 34 T while a strong enhancement occurs for the components smaller than 30 T. As for the previous sample, these modifications indicate the destroying of the bcc iron layers due to the progressive thickening of the interfaces. The mean hyperfine field $\langle B_{hf}\rangle$ decreases slowly and continuously when the Xe ions fluence increases (Fig. 8) and it would tend towards the value of the amorphous alloy at the same composition (18 T for 20 at. % Tb).[17,18] Moreover, iron magnetic moments rotate towards the plane with the fluence (initially $\beta=70°$, after 8×10^{12} ions Xe cm^{-2}, $\beta=84°$) (Fig. 9). In addition to the thickening of the Fe-Tb interfaces which reduces the perpendicular anisotropy, enough α-iron still exists in the center of the Fe layers to impose a planar anisotropy.

C. Discussion

To summarize, for the $S1$ sample, we evidenced three structural changes. An additional crystallization leading to thicker bcc Fe layers is observed in the whole range of the Kr fluences (up to 1.6×10^{13} ions/cm^2) and for small fluences of Xe and Pb ions. At higher fluences, the mixing of the Fe and Tb layers is observed for every type of ion, except for the Kr ion. The bombardment with heavy ions (Pb and U) produces the growing of a new weakly magnetic phase different from the amorphous Fe-Tb alloy state. For the $S2$ sample irradiated with Xe ions at small fluences, only the mixing process between the layers is evidenced.

From the kinetics of the α-iron transformation, the energy deposition process of ions in matter can be determined for the two samples. If we assume that the observed structural and magnetic changes occur along continuous ion tracks with an effective cross section A, one can write $dF/d\phi = A(1-F)$ where ϕ is the ion fluence and F is the transformed fraction of iron calculated from the initial state of the ML's, i.e., either the bcc Fe part which becomes disordered or the fraction of disordered iron which changes into the bcc

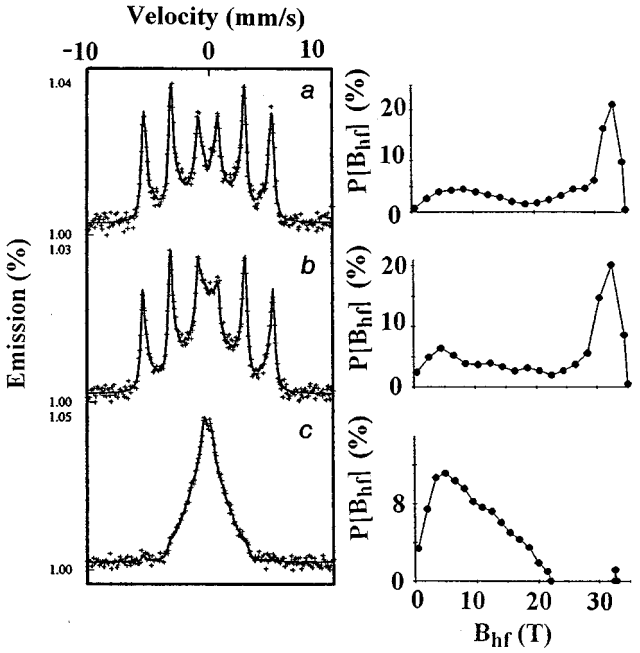

FIG. 6. Mössbauer spectra and $P(B_{hf})$ for the $S1$ sample at 300 K irradiated with U ions: (a) nonirradiated; (b) 5.2×10^{11} ions/cm^2; (c) 1.76×10^{12} ions/cm^2.

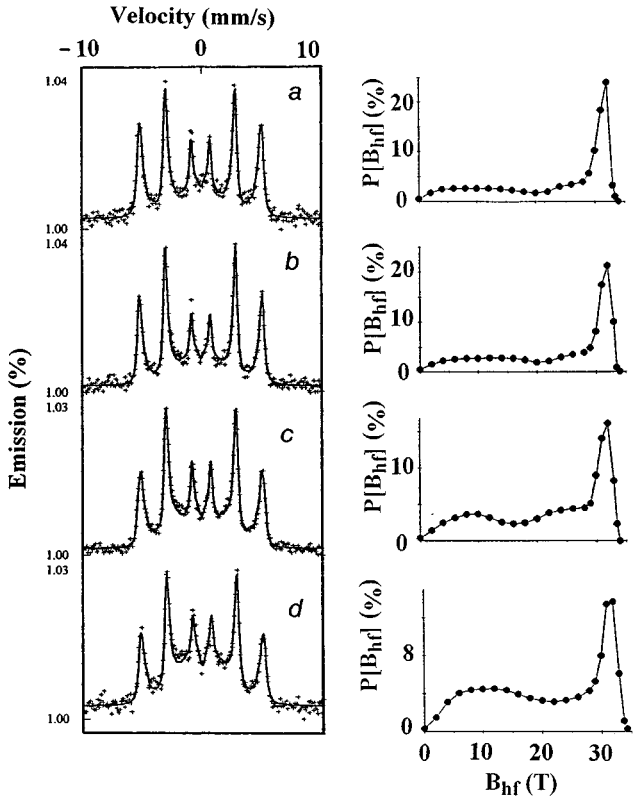

FIG. 7. Mössbauer spectra and $P(B_{\mathrm{hf}})$ at 300 K for the $S2$ sample irradiated with Xe ions: (a) nonirradiated; (b) 2×10^{12} ions/cm^2; (c) 4×10^{12} ions/cm^2; (d) 8×10^{12} ions/cm^2.

structure. The parameter F can be easily deduced from the fitted relative fraction of Fe atoms in the bcc iron phase $A_{\alpha\text{-Fe}}$ (Table II).

First, let us discuss the results for the $S1$ sample. To obtain a striking view of the different processes, the noncrystalline part of iron is plotted versus $\ln(\phi)$ (Fig. 10). The additional crystallization of the bcc iron layers is clearly pointed out by the part of the curves which exhibits a negative slope and the amorphization processes, including the mixing of layers and the growing of the weakly magnetic phase, are relative to a positive slope. The obtained straight lines confirm that the creation of defects occurs by excitation of the electrons of the target in the ion path, which means by a statistical deposition along the tracks of ions. It is noteworthy that the points deduced from the Pb and U irradiation experiments are located on the same curve agreeing with their closely lying values of $(dE/dx)_e$.

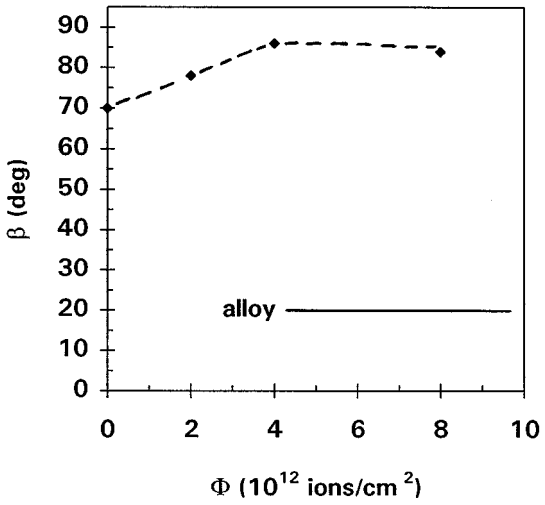

FIG. 9. The mean Mössbauer angle β as function of the Xe ion fluence for $S2$.

Because of the relation $F(\phi)=1-\exp(-A\phi)$, the slope of the representation $-\ln(1-F)$ versus the ion fluence ϕ (Fig. 11) allows one to determine the effective cross-section A and the effective radius R of the latent tracks in the hypothesis of continuous tracks. The deduced values are listed in Table III.

As far as the Kr ions are concerned, the straight line has a negative slope (Fig. 11) because the bcc Fe fraction increases with the fluence. The straight line effectively goes through the origin of the diagram because the extra-crystallization step begins from the nonirradiated multilayer. In this case,

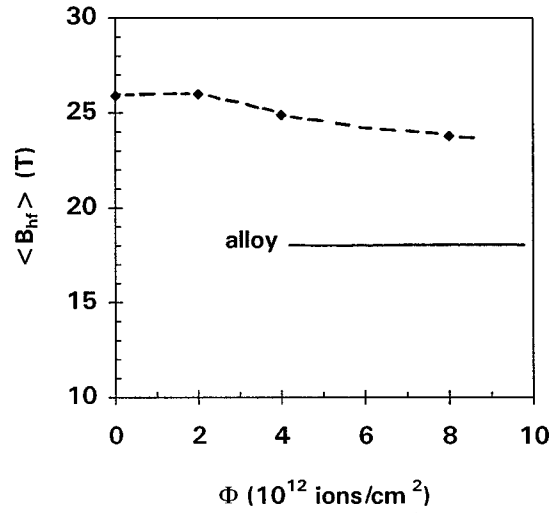

FIG. 8. $\langle B_{\mathrm{hf}}\rangle$ vs the Xe ion fluence for the $S2$ sample.

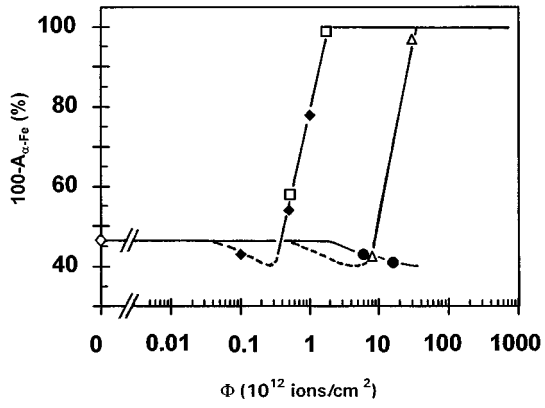

FIG. 10. Percent of disordered iron $(100-A_{\alpha\text{-Fe}})$ in the $S1$ sample as function of the ion fluence: nonirradiated (◇), Kr (●), Xe (△), Pb (◆), and U (□).

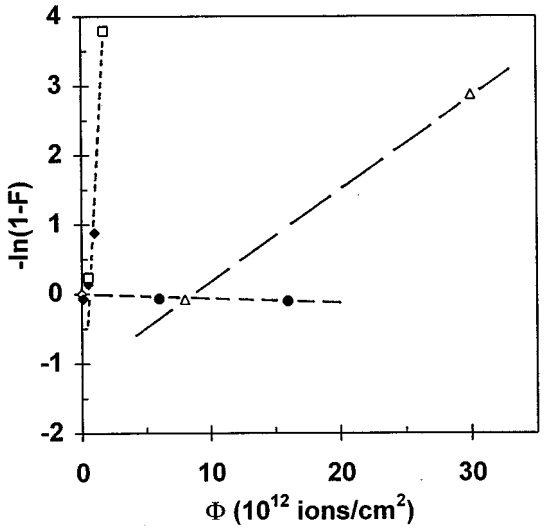

FIG. 11. $-\ln(1-F)$ vs the ion fluence for the $S1$ sample irradiated with nonirradiated (◇), Kr (●), Xe (△), Pb (◆), and U (□).

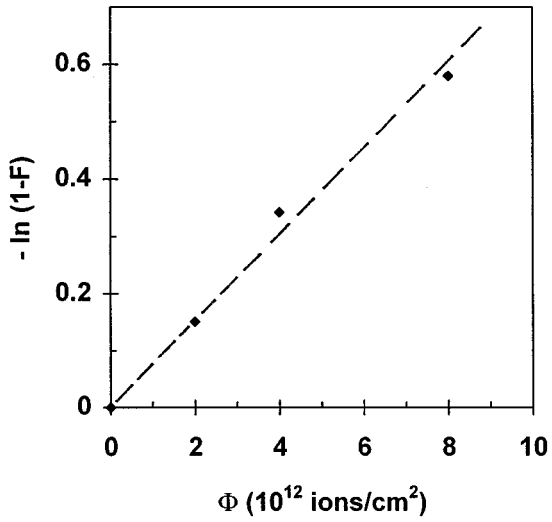

FIG. 12. $-\ln(1-F)$ vs the Xe ion fluence for the $S2$ sample.

where the Fe-Tb demixing process occurs alone, the deduced track radius actually corresponds to an effective demixing track radius.

For the other ions (Xe, Pb, and U), the lack of points at the lowest fluences does not allow one to study the demixing process and only the points relative to the mixing of layers or the weakly magnetic phase growing were considered, i.e., the points belonging to the linear part with a positive slope (Fig. 10). According to what was previously seen, the points relative to Pb and U irradiations are lying along the same straight line.

In contrast to what was observed until now, the straight lines relative to the Xe, Pb, and U ion bombardments do not intersect the origin of the diagram which corresponds to the nonirradiated multilayer (Fig. 11). This is a signature of the additional crystallization of the iron layers which occurs at small fluences and changes the initial state of the ML's before the further transformations.

The slope of the straight lines allows one to determine the effective radii of the continuous tracks corresponding to the mixing of layers for the Xe ion irradiation, and to the mixing of layers added to the weakly magnetic phase appearance for the bombardment with the heaviest ions (Pb and U). As expected, the values of the effective tracks radii increase with the electronic stopping power of the ions. The higher-value obtained for the Pb and U ion irradiations (Table III) compared to those obtained on (bcc Fe/Si) multilayers[8] and on pure bcc Fe (Ref. 19) irradiated with U ions can be attributed to the two simultaneous processes which occur in these Fe/Tb ML's.

TABLE III. Effective cross section A and effective radius R of the tracks assumed to be continuous for $S1$ irradiated with different ions.

Ions	A (nm^2)	R (nm)
Kr	0.25	0.3
Xe	13.3	2.1
Pb	287	9.5
U	287	9.5

The damage evolution described by the law $-\ln(1-F)=A\phi$ for the $S2$ sample is reported in Fig. 12. The best fit gives an effective cross section $A=7.5$ nm^2 which means an effective radius of track $R=1.54$ nm. The discrepancy with the previous value obtained for the $S1$ sample irradiated with Xe ions ($R=2.1$ nm) is due to the hypothesis of the continuous tracks, the smaller radius value corresponding to the thicker (Fe/Tb) bilayer. In striking contrast with the previous multilayer, the straight line intersects the origin. Thus, the additional crystallization of the iron layers at small fluence does not occur.

We will now interpret the different observed damaging processes. Let us recall that increasing the ion deposited energy, and increasing the fluences, we showed that the ion irradiation of these Fe/Tb crystallized multilayers can exhibit three phenomena: a demixing between the atoms, a mixing of layers and the appearance of a weakly magnetic phase.

The mixing of layers is a commonly observed effect on multilayers[8,11] and confirms the initial layered structure of the samples. With the assumption that it starts from the interfaces, this process produces in a first step a progressive thickening of the interfaces and finally destroys the layered structure. Thus, the samples exhibit structural and magnetic properties which tend towards those of the amorphous alloys at the same global composition. As for the amorphous Fe/Tb ML's,[11] the defect creation causing this mixing does not occur for the Kr ions, even at the highest fluence, but it is observed during the Xe, Pb, and U bombardments. So, the damage creation threshold for mixing of the iron and terbium atoms appears only above a critical value of the electronic stopping power, which is estimated between 17 and 32 keV/nm which are, respectively, the electronic stopping powers for the Kr and Xe ions (Table I). Above this threshold, the mixing of the Fe-Tb atoms will occur in the ion tracks because the deposited energy has reached the mixing energy value.

For the $S1$ multilayer, an additional crystallization of iron is first observed for all types of ions. We explain it by a

demixing of Fe and Tb atoms at the interfaces. This segregation increases the pure iron part, which is initially in the center of the iron layers of the sample and sharpens the interfaces. So, the defects are created at the boundary of the Fe/Tb and Tb/Fe interfaces. Thus, in the layered structure of the multilayers, a supplementary discontinuity of the tracks is introduced as compared to the usual one produced by the statistical energy deposition.

In contrast to the mixing, this demixing process occurs for the four types of studied ions, but it occurs in a fluence range which decreases when the electronic stopping power of the ions becomes larger, because the fluence needed to start the mixing process decreases when the $(dE/dx)_e$ value increases. If there is a threshold of demixing, it is less than 17 keV/nm.

This demixing process does not appear for the $S2$ multilayer, which contains thicker bcc iron layers before irradiation. This means that the demixing of Fe and Tb atoms at the interfaces occurs only for the multilayers located near the crystallization limit of the bcc Fe layers. It could originate from a structural metastability of the ML's near this transition zone, related to the preparation process. This Fe and Tb demixing process would correspond to a structural relaxation of the system, the equilibrium solubility of Fe into Tb or of Tb into Fe being inferior to one atomic percent,[20] because of a strong positive heat of mixing between Fe and Tb. A similar demixing process due to stress relaxation was observed on laser-deposited Fe/Ag multilayers irradiated with low-energy ions (350 keV Ar^+).[21] Up to now, only one observation of induced crystallization by ion bombardment was evidenced.[22] In initially amorphous W/Si multilayers, a new crystallized WSi compound was observed after high-energy heavy-ion (^{127}I and ^{238}U) irradiations, but this did not separately concern the W or Si layers.

The weakly magnetic phase, which appears by irradiation with heavy ions (Pb,U) is similar to what is observed near the critical thickness of crystallization of the iron layers in nonirradiated amorphous multilayers, which contain a large thickness of «pure» amorphous iron in the center of the Fe layers.[9–11]

This result suggests a damage creation in the center of the bcc iron layers without mixing between the Fe and Tb atoms and is in agreement with the values of the electronic stopping powers of the Pb and U ions (Table I) which exceed the defect creation threshold in the bulk bcc iron (40 keV/nm).[23] In this case, the damages created along the tracks would disorder the center of the bcc iron layers producing a phase of ''pure'' amorphous iron at room temperature. This phase has a Curie temperature, T_C, close to 200 K and is paramagnetic at 300 K,[11,24] agreeing with what is observed here.

These ions (Pb and U) are likely included in the energetic domain where the latent tracks are continuous along the ion path with defect creation at the interfaces (demixing or mixing) and also in the center of the Fe layers. This allows one to explain the strong decrease of the mean Mössbauer angle after the U irradiation at the highest fluence (Table II). First, the demixing process produces a sharpening of the interfaces, and so increases the PMA. Second, the amorphization of the iron layers producing a paramagnetic phase in the center of the iron layers yields the decrease of the demagnetizing field, and so the vanishing of the planar anisotropy. So, finally, the perpendicular magnetic anisotropy is enhanced.

Because the progressive mixing of the layers by U ions seems to continue during the amorphization of the iron layers, the final state of the samples, at higher fluences, would be a homogeneous amorphous Fe-Tb alloy.

As previously mentioned, the kind of the created damages depends not only on the electronic energy deposition but also on the ion fluence.

This dependence with the ion fluence, when the $(dE/dx)_e$ value of ions is larger than the threshold value for Fe-Tb mixing or for defect creation in bcc Fe, could be explained by the thermal spike model:[25] the melting point being reached in the middle of the tracks would lead to the mixing or the amorphization of the bcc iron, while, outside the tracks where the temperature is lower, only the demixing would occur. Increasing the ion fluence, the number of tracks also increases and the part of mixing would increase. To confirm this assumption, further experiments are in progress to determine precisely the $(dE/dx)_e$ value corresponding to the Fe-Tb mixing and to estimate the activation energy leading to the demixing process.

IV. CONCLUSION

In irradiated (bcc Fe/Tb) multilayers, three structural effects are evidenced: the demixing of Fe and Tb atoms at the interfaces, the mixing of layers, and the creation of defects in the core of the bcc iron layers. The first process leads to an increase of pure Fe in the center of iron layers producing a sharpening of the interfaces, while the second destroys progressively the layered structure and leads to the formation of the corresponding amorphous alloy at high fluence. The electronic stopping power threshold of Fe-Tb mixing has been estimated between 17 and 32 keV/nm. The demixing process, observed only at low fluence before the step of mixing for the multilayer close to the thickness limit of crystallization of the Fe layers, features the structural metastability of this multilayer. The third phenomenon occurs only above the defect creation threshold in bulk bcc iron and induces the appearance of a paramagnetic phase at room temperature which corresponds to the ''pure'' amorphous iron in the center of Fe layers. The improvement of the PMA in these ML's is obtained because of the sharpening of the interfaces which increases the PMA and the partial amorphization of the bcc Fe layers which produces a vanishing of the planar magnetic anisotropy due to the decreasing demagnetizing field. To explain the evolution versus the ion fluence, a qualitative interpretation has been proposed using the thermal spike model.

ACKNOWLEDGMENTS

The authors would like to thank Philippe Houdy from the University of Evry (France) for providing the samples, Emmanuel Balanzat for helpful discussion, and Jacques Dural and Francis Levesque for their efficient help during the irradiation experiments (GANIL, France).

[1] P. Hansen, H. Heitmann, and P. H. Smit, Phys. Rev. B **26**, 3539 (1982).
[2] S. Klaumünzer, H. Ming-Dong, and G. Schumacher, Phys. Rev. Lett. **57**, 850 (1986).
[3] A. Audouart, E. Balanzat, G. Fuchs, J. C. Jousset, D. Lesueur, and L. Thome, Europhys. Lett. **3**, 327 (1987).
[4] M. Toulemonde and F. Studer, Philos. Mag. A **58**, 799 (1988).
[5] A. Barbu, A. Dunlop, D. Lesueur, and R. S. Averback, Europhys. Lett. **15**, 37 (1991).
[6] M. Toulemonde, G. Fuchs, N. Nguyen, F. Studer, and D. Groult, Phys. Rev. B **35**, 6560 (1987).
[7] D. Givord, J. P. Nozieres, M. Ghidini, B. Gervais, and Y. Otani, J. Appl. Phys. **76**, 6661 (1994).
[8] C. Dufour, Ph. Bauer, G. Marchal, C. Jaouen, J. Pacaud, and J. C. Jousset, Europhys. Lett. **21**, 671 (1993).
[9] F. Richomme, J. Teillet, A. Fnidiki, P. Auric, and Ph. Houdy, Phys. Rev. B **54**, 416 (1996).
[10] F. Richomme, J. Teillet, P. Auric, P. Veillet, A. Fnidiki, Ph. Houdy, and P. Boher, J. Magn. Magn. Mater. **140**, 627 (1995).
[11] F. Richomme, A. Fnidiki, J. Teillet, and M. Toulemonde, Nucl. Instrum. Methods B **107**, 374 (1996).
[12] S. Bouffard, J. Dural, F. Levesque, and J. M. Ramillon, Ann. Phys. (Paris) **4**, 395 (1989).
[13] J. P. Biersack and L. G. Haggmark, Nucl. Instrum. Methods **174**, 257 (1980).
[14] J. Teillet and F. Varret, unpublished MOSFIT program.
[15] F. Varret, A. Gerard, and P. Imbert, Phys. Stat. Solidi B **43**, 723 (1971).
[16] F. Richomme, B. Scholz, R. A. Brand, W. Keune, and J. Teillet, J. Magn. Magn. Mater. **156**, 195 (1996).
[17] V. S. Rusakov, B. S. Vvedensky, E. T. Voropaeva, and E. N. Nikolaev, IEEE Trans. Magn. **28-2**, 2524 (1992).
[18] V. S. Rusakov, B. S. Vvedensky, S. N. Gadetsky, E. T. Voropaeva, V. V. Kochetov, A. V. Stupnov, and E. N. Nikolaev, J. Magn. Soc. Jpn. **17-S1**, 35 (1993).
[19] A. Dunlop, D. Lesueur, J. Morillo, J. Dural, R. Spohr, and J. Vetter, Nucl. Instrum. Methods B **48**, 90 (1990).
[20] O. Kubaschewski, *Iron Binary Phase Diagrams* (Springer-Verlag, Berlin, 1982), p. 108.
[21] H. U. Krebs, Y. Luo, M. Störmer, A. Crespo, P. Schaaf, and W. Bolse, Appl. Phys. A **61**, 591 (1995).
[22] J. Marfaing, W. Marine, B. Vidal, M. Toulemonde, M. Hage-Ali, and J. P. Stoquert, Appl. Phys. Lett. **57**, 1739 (1990); Appl. Surf. Sci. **46**, 422 (1990).
[23] A. Dunlop, D. Lesueur, P. Legrand, H. Dammak, and J. Dural, Nucl. Instrum. Methods **90**, 330 (1994).
[24] J. J. Rhyne, IEEE Trans. Mag. **MAG-21**, 1990 (1985).
[25] M. Toulemonde and C. Dufour, Phys. Rev. B **42**, 14 362 (1992).